New Physics: Sae Mulli,
Vol. 68, No. 3, March 2018, pp. 290∼295
http://dx.doi.org/10.3938/NPSM.68.290

Rod-Shaped Dextran-Coated Nickel-Ferrite Nanoparticles for Use as Contrast Agents in Magnetic Resonance Imaging

Da-Ae Lee · Yusaf Iqbal · Hongsub Bae · Ilsu Rhee*
Department of Physics, Kyungpook National University, Daegu 41566, Korea

Sungwook Hong
Division of Science Education, Daegu University, Gyeongsan 38453, Korea

(Received 15 December 2017 : revised 14 January 2018 : accepted 6 February 2018)

Rod-shaped nickel-ferrite ($NiFe_2O_4$) nanoparticles were synthesized using a coprecipitation method and were coated with dextran during the synthesis. Transmission electron microscope (TEM) images showed that the average length and width of these particles were 16.86 nm and 3.92 nm, respectively. The coating status of the dextran on the surface of the particles was confirmed by using Fourier-transform infrared spectroscopy. X-ray diffraction measurements showed that the particles had a spinel crystalline structure. The paramagnetic behavior of the particles provided the contrast effects in magnetic resonance imaging (MRI). The T_1 and the T_2 relaxivities were 2.05 $mM^{-1}{\cdot}s^{-1}$ and 4.92 $mM^{-1}{\cdot}s^{-1}$, respectively. The T_2 relaxivity was more than twice the T_1 relaxivity. However, the T_1 relaxivity value was still appropriate for the application of these particles as T_1 contrast agents. These findings show that the rod-shaped particles fabricated in this research can be employed as both T_1 and T_2 MRI contrast agents.

PACS numbers: 75.20.-g, 81.05.-t, 75.50.Tt, 76.60.-k
Keywords: Nickel-ferrite nanoparticles, Dextran coating, Magnetic resonance imaging contrast agents

I. INTRODUCTION

Magnetic nanoparticles attract significant research interests, in particular, for biomedical applications where they can act as contrast agents in magnetic resonance imaging (MRI) [1,23], carriers in targeting drug delivery systems [4–6], heat generators in a magnetic hyperthermia [7–9], *etc.* Commercial nanoparticle contrast agents are currently used for clinical applications. Several clinical applications of magnetic nanoparticles for a hyperthermia treatment of cancer have been reported [10–12]. Various magnetic nanoparticles are studied for applications in targeting drug delivery systems.

Ferrite nanoparticles are extensively investigated for biomedical applications. Ferrite has the chemical composition of MFe_2O_4, where M is a metallic cation such as Fe^{2+}, Mn^{2+}, Co^{2+}, Ni^{2+}, *etc.* Among various forms of ferrites, the iron ferrite (magnetite, Fe_3O_4) nanoparticles have been widely used in biomedical applications owing to their simple synthesis and chemical stability. Other ferrites are investigated for specific applications owing to their tailored characteristics. The ferrite has a cubic crystalline structure where 32 O^{2-} ions form a face centered cubic (FCC) structure, 8 tetrahedral sites are occupied by Fe^{3+}, 8 of the 16 octahedral sites are occupied by M^{2+}, while the other 8 octahedral sites by Fe^{3+} ions. The directions of the magnetic moments of Fe^{3+} at tetrahedral sites and Fe^{+3} at octahedral sites are antiparallel, hence their magnetic moments are cancelled out. Therefore, the magnetic moment of ferrite is attributed to the M^{2+} ions. The ferrite has an inverse spinel crystalline structure [13,14].

Most of the magnetic nanoparticles are toxic, hence they cannot be directly used in a human body. For medical applications, the surface of the particle should be

*E-mail: ilrhee@knu.ac.kr

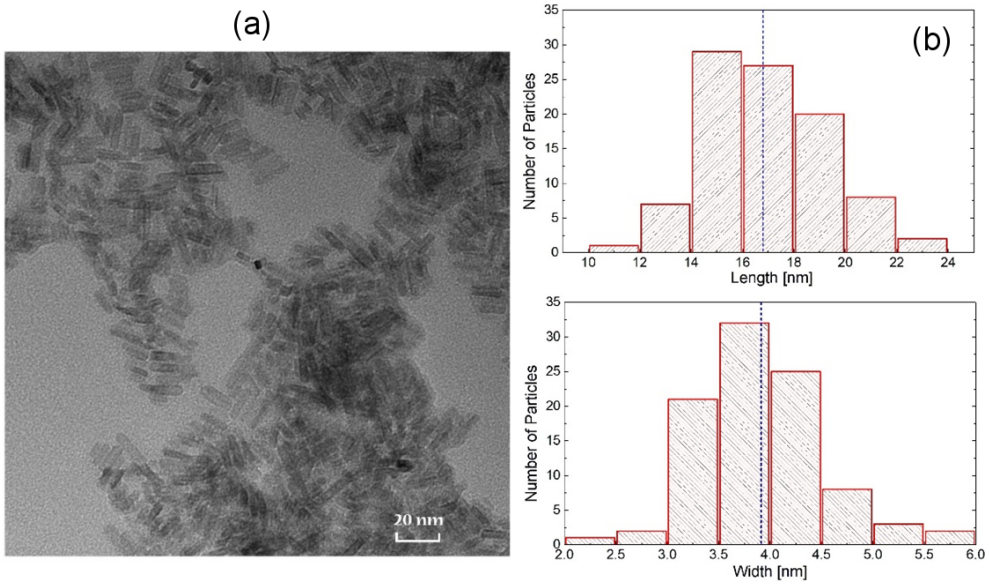

Fig. 1. (Color online) (a) TEM image and (b) particle size distribution of the dextran-coated nickel-ferrite nanoparticles.

coated with a biocompatible material. Various materials are studied for the coating of magnetic nanoparticles, such as dextran [15,16], chitosan [17], silica [18], carbon [19], gold [20,21], *etc.*

We report the synthesis and characterization of dextran-coated nickel-ferrite nanoparticles for potential applications as contrast agents in MRI. The particles were rod-shaped and exhibited a paramagnetic behavior, caused by their shape anisotropy. The function of the particles as contrast agents was observed using an MRI scanner. The T_1 and T_2 relaxivities of the particles were determined using magnetic resonance (MR) images, which demonstrated that their relaxivities were comparable to those of a commercial Gd-DTPA. This reveals that the proposed rod-shaped dextran-coated nickel-ferrite nanoparticles could be employed as MRI contrast agents.

II. EXPERIMENTAL METHODS

The rod-shaped nickel-ferrite nanoparticles were synthesized using the coprecipitation method. The surfaces of the nanoparticles were coated with dextran simultaneously during their synthesis. First, 3 ml of 0.3 M $NiCl_2{\cdot}4H_2O$ aqueous solution was mixed with 3 ml of 0.6 M $FeCl_3{\cdot}6H_2O$ aqueous solution. Then, 6 ml of 2% (w/w) dextran solution was added to this mixture in a 250 ml double walled beaker. The temperature of the circulating water across the double walled beaker was maintained at 4 °C. Air bubbles were introduced into the mixture using a pipette for 1 h. During the formation of nanoparticles, dextran adheres to the surface of the particles at a PH of around 7. In order to achieve this condition, 1% (v/v) NaOH was added dropwise to the reaction mixture at a rate of 1 mL/min. In order to stabilize the nanoparticles, the final solution was placed in an ultrasonic environment for 10 h, followed by a filtration using a 100 nm filter. The size of the nanoparticles depends on the ultrasonic treatment time, as the ultrasonic treatment provides an energy to dissociate the excessive dextran from the coated particles. A coated nanoparticles powder sample was obtained by placing the wet particles in an air environment at a temperature of 70 °C for approximately 12 days.

Crystallinity and phase purity were investigated by X-ray diffraction (XRD, X'pert PRO, PANalytical) in order to confirm the spinel structure of the nanoparticles. A chemical composition analysis was performed using inductively coupled plasma spectroscopy (ICP, IRISAP, Thermo Jarrell Ash). The shape and size of the nanoparticles were investigated using a transmission electron microscope (TEM, HT 7700, Hitachi Ltd). Fourier transform infra-red spectroscopy (FTIR, Nicolet 380, Thermo Scientific USA) measurements were performed in order

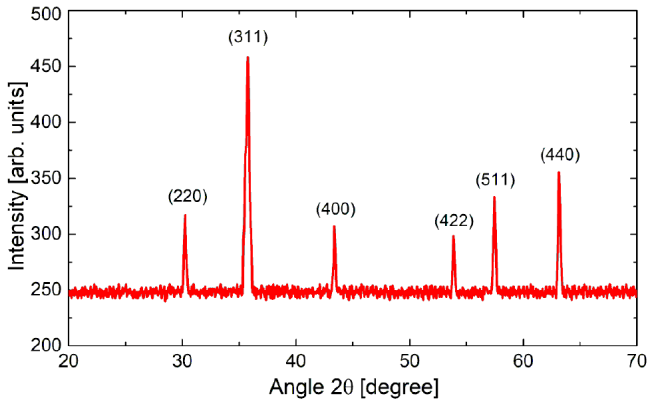

Fig. 2. (Color online) XRD patterns of the dextran-coated nickel-ferrite nanoparticles. The indices of the crystal planes in the figure match with those of an inverse spinel ferrite.

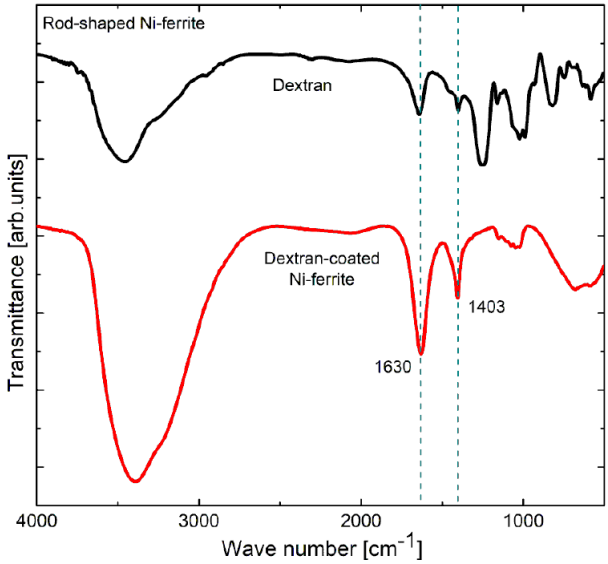

Fig. 3. (Color online) FTIR spectra of a pure dextran and dextran-coated nickel-ferrite nanoparticles. The absorption bands correspond to the stretching and vibration modes of specific chemical bonds.

to evaluate the status of the coating. Magnetic properties of the particles were measured using a SQUID magnetometer (MPMS XL 7, Quantum Design). MRI contrast effects were observed using a 4.7 T MRI System (Bruker Biospec 47/40).

III. RESULTS AND DISCUSSION

Fig. 1 shows a TEM image and size distribution of the rod-shaped nickel-ferrite nanoparticles. An average length and width of 16.86 nm and 3.92 nm, respectively, were determined. These size values were obtained using histograms of 100 particles observed in the TEM image.

The crystalline structure of the particles was observed using X-ray diffraction. XRD patterns for the particles are shown in Fig. 2. The particles showed a spinel crystalline structure; the crystalline indices of (220), (311), (400), (422), (511), and (422) were identified in the XRD patterns [JCPDS No. 10-3025].

The coating status of dextran on the surfaces of the nickel-ferrite nanoparticles was studied using FTIR spectroscopy, as shown in Fig. 3. This figure shows the comparison of FTIR spectra of dextran and dextran-coated nickel-ferrite nanoparticles. The absorption bands at 1600 cm^{-1} and 3400 cm^{-1} correspond to the O-H stretching mode of the hydroxyl group and O-H deformation mode of the water molecules, respectively. The C-O vibration mode of dextran corresponds to the band in the range of 1040 $\sim$ 1150 cm^{-1}. The bands at 1630 cm^{-1} and 1403 cm^{-1} emerge from the O-H stretching and C-H vibration modes of dextran, respectively. The absorption strengths of these bands are almost equal. However, the absorption strength of the O-H stretching mode for the dextran-coated particles is larger than that of the C-H vibration mode, which can be attributed to the hydrogen bonding between the surface oxygen and hydroxyl of the dextran [22,23]. The FTIR spectra demonstrate the dextran coating on the particles' surfaces.

The magnetic properties of the particles were measured using a SQUID system. The dependence of the magnetization as a function of the field strength is shown in Fig. 4. The magnetic particles showed a paramagnetic behavior with a curved structure near zero field owing to the large anisotropy along the length direction, which is shown in references [24,25].

The T_1 and T_2 relaxation times of the nuclear spins (hydrogen protons) in the aqueous solution of magnetic nanoparticles were measured using an MR scanner. For these measurements, ten samples with different particle concentrations, ranged from 0.025 mM to 2 mM, were prepared. The particle concentration in the solution was determined using an ICP spectroscopy.

The spin-lattice relaxation time T_1 mainly depends on the rate of energy transfer from the nuclear spins to the neighboring molecules. However, the spin-spin relaxation time T_2 depends on the dephasing process of

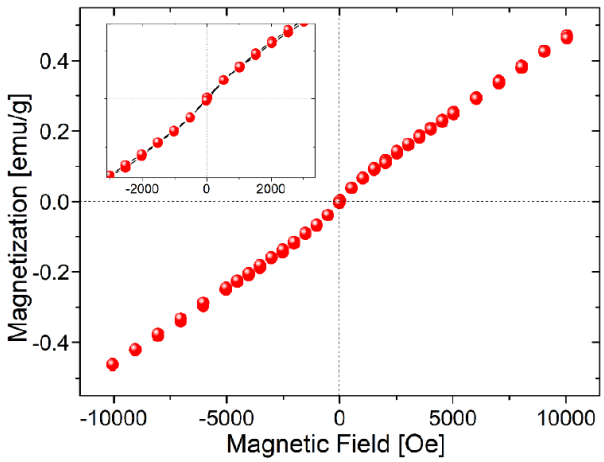

Fig. 4. (Color online) Magnetic moment of the nanoparticles as a function of the applied magnetic field. The particles exhibit a paramagnetic behavior owing to their shape anisotropy.

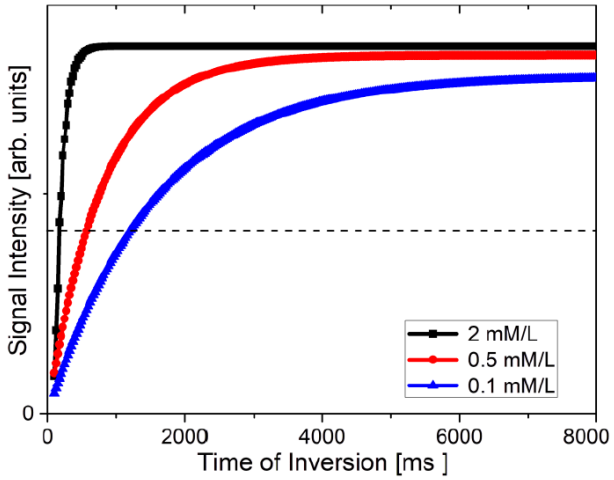

Fig. 5. (Color online) T_1 relaxation for three representative samples. The dotted line represents the zero MR signal intensity. It can be noticed that the T_1 relaxation is faster for the sample that has a larger particle concentration.

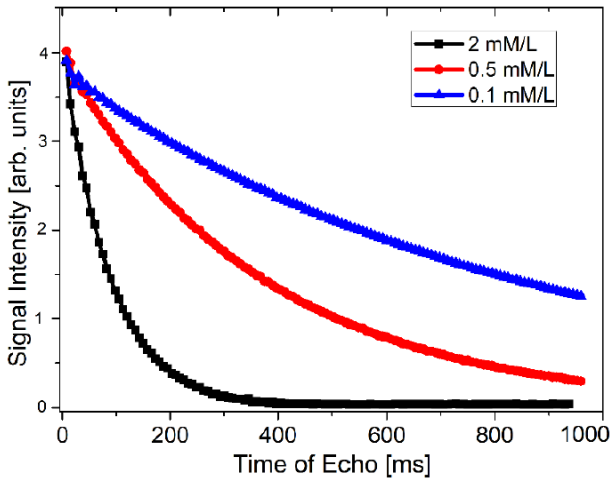

Fig. 6. (Color online) T_2 relaxation for three representative samples. It can be noticed that the T_2 relaxation is faster for the sample that has a larger particle concentration.

the nuclear spins caused by the neighboring magnetic inhomogeneity. The T_1 and T_2 relaxation times of the nuclear spins in a pure water are equal and have a value of approximately 3 s. The nuclear spins of a human tissue have different relaxation times that depend on its water content and surroundings. The relaxation times of the nuclear spins in a certain tissue are decreased by the introduction of magnetic particle contrast agents. If MRI contrast agents (an aqueous solution of magnetic particles) are injected into human body, these particles are absorbed only by normal tissues [14]. Owing to the lack of reticuloendothelial systems in cancer tissues, they have no capability to capture the nanoparticles by recognizing them as external invaders. A T_1 contrast agent increases the T_1 relaxation at a normal tissue site, which increases the signal from that site and provides a brighter image compared with that of the cancer site. On the other hand, a T_2 contrast agent accelerates the T_2 relaxation at a normal tissue, which decreases the MR signal at that site, while the MR signal at the cancer site remains unaltered. Therefore, a T_2 agent can be used to distinguish between the cancer and normal tissues.

For the T_1 measurements, an inversion recovery pulse sequence was used. In this sequence, the signal intensities as a function of time can be expressed as:

$$I \sim M_0 \left(1 - 2e^{-\frac{t}{T_1}}\right) . \qquad (1)$$

Using the MR intensities and Eq. (1), we can obtain the T_1 relaxation time, as shown in Fig. 5 for samples that have three different representative particle concentrations.

The Carr-Purcell-Meiboon-Gill (CPMG) pulse sequence with a multiple spin echo was used for the T_2 measurements. The signal intensity is related to the T_2 relaxation time:

$$I \sim M_0 e^{-\frac{t}{T_2}} , \qquad (2)$$

which was used to determine the value of the T_2 relaxation time. Fig. 6 shows the T_2 relaxation for samples that have three different representative particle concentrations.

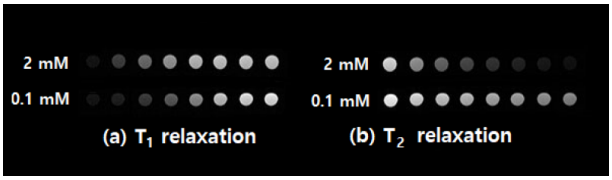

Fig. 7. (Color online) MR images show the T_1 and T_2 relaxation processes as a function of the imaging time for two representative samples. It can be noticed that the relaxation process is faster for the sample that has a higher particle concentration.

MR images of samples that have two representative particle concentrations of 2 mM and 0.1 mM are shown in Fig. 7, where from left to right the imaging time increases. In a T_1 relaxation, the MR images of both samples become brighter with the imaging time. However, the MR image of the 2 mM sample becomes brighter, much faster compared with the 0.1 mM sample. On the other hand, in a T_2 relaxation, the MR images of both samples become darker with the imaging time. However, the MR image of the 2 mM sample becomes darker much faster compared with the 0.1 mM sample.

Relaxivity is a measure of the ability of the MRI contrast agent to increase the relaxation of the surrounding nuclear spins, which can be used to improve the contrast of the MR images. The relaxivity is expressed in units of s^{-1}/mM (of nanoparticles).

The relaxivities $(1/T_{im})$ of nuclear spins in an aqueous solution of magnetic nanoparticles can be expressed as [26]:

$$\frac{1}{T_{im}} = \frac{1}{T_i} + R_i C \ , \qquad (3)$$

where $i = 1$ or 2, $1/T_i$ represent the relaxivities of the nuclear spins without a nanoparticle contrast agent, R_i are the relaxivities of the nuclear spins per millimolar of nanoparticles, and C represents the concentration of nanoparticles in the aqueous solution.

The dependence of both $1/T_1$ and $1/T_2$ as a function of the particle concentration are shown in Fig. 8. In this figure, the slope reveals the relaxivity values. It was determined that the T_1 and T_2 relaxivities are 2.05 $mM^{-1}{\cdot}s^{-1}$ and 4.92 $mM^{-1}{\cdot}s^{-1}$, respectively. The T_1 and T_2 relaxivities of the commercial paramagnetic contrast agent Magnevist (Gd-DTPA) are 4.3 $mM^{-1}{\cdot}s^{-1}$ and 4.4 $mM^{-1}{\cdot}s^{-1}$, respectively [14]. However, the commercial spherical nanoparticles contrast agent Feridex IV shows

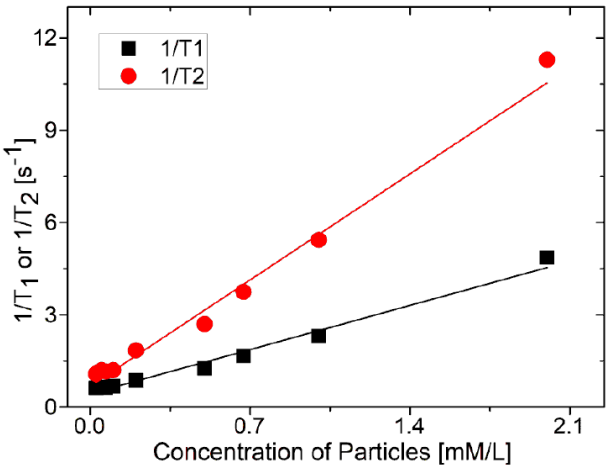

Fig. 8. (Color online) Dependence of $1/T_1$ and $1/T_2$ as a function of the particle concentration. The slope of the straight line reveals the T_1 and T_2 relaxivities of the nanoparticles.

a significantly larger T_2 relaxivity of approximately 60 $mM^{-1}{\cdot}s^{-1}$, owing to the large particle size and superparamagnetic behavior [14]. Our dextran-coated nickel-ferrite nanoparticles showed a similar relaxivity, compared with that of the commercial paramagnetic agent Gd-DTPA. Therefore, the particles can be employed as both T_1 and T_2 MRI contrast agents.

IV. CONCLUSION

Nickel-ferrite nanoparticles were synthesized using a coprecipitation method. Dextran coating was performed on the surface of the particles during their synthesis. TEM measurements showed that the particles are rod-shaped. The average length and width of the particles were 16.86 nm and 3.92 nm, respectively. Using FTIR spectroscopy, we confirmed the presence of dextran coating on the surface of the particles. The particles showed a paramagnetic behavior owing to their shape anisotropy. In addition, XRD measurements demonstrated the spinel crystalline structure of the particles. The function of the particles as T_1 and T_2 contrast agents was evaluated using an MRI scanner. The T_1 and T_2 relaxivities were obtained as 2.05 $mM^{-1}{\cdot}s^{-1}$ and 4.92 $mM^{-1}{\cdot}s^{-1}$, respectively. The T_1 and T_2 relaxivities were comparable with those of the commercial Gd-DTPA. Therefore, we can conclude that our particles are suitable for applications as both T_1 and T_2 MRI contrast agents.

ACKNOWLEDGMENTS

This research was supported by the National Research Foundation of Korea (2016R1A2B1006449).

REFERENCES

[1] D. Pouliquen, J. J. Le Jeune, R. Perdrisot, A. Ermias and P. Jallet, Magn. Res. Imaging **9**, 275 (1991).

[2] T. Ahmad, H. Bae, I. Rhee, Y. Chang and J. Lee *et al.*, Curr. Appl. Phys. **12**, 969 (2012).

[3] T. Ahmad, H. Bae, Y. Iqbal, I. Rhee and S. Hong *et al.*, J. Magn. Magn. Mater. **381**, 151 (2015).

[4] M. Liong, J. Lu, M. Kovochih, T. Xia and S. G Ruehm *et al.*, ACS Nano **2**, 889 (2008).

[5] J. Dobson, Drug. Dev. Res. **67**, 55 (2006).

[6] R. D. K. Misra, Mater. Technol.: Adv. Perform. Mater. **25**, 118 (2010).

[7] H. S. Huang and J. F. Hainfeld, Int. J. Nanomed. **8**, 2521 (2013).

[8] Y. Iqbal, H. Bae, I. Rhee and S. Hong, J. Magn. Magn. Mater. **409**, 80 (2016).

[9] A. Ahmad, H. Bae, I. Rhee and S. Hong, J. Magn. Magn. Mater. **447**, 42 (2018).

[10] R. D. Tucker, C. E. Platz, C. Huidobro and T. Larson, Urology **60**, 166 (2002).

[11] B. Thiesen and A. Jordan, Int. J. Hyperthermia **24**, 467 (2008).

[12] T. Kobayashi, K. Kakimi, E. Nakayama and K. Jimbow, Nanomedicine **9**, 1715 (2014).

[13] B. D. Cullity and C. D. Graham, *Introduction to Magnetic Materials*, 2nd ed. (John Wiley & Sons, 2011).

[14] I. Rhee, New Phys.: Sae Mulli **65**, 411 (2015).

[15] T. Ahmad, H. Bae, I. Rhee, S. Hong and Y. Chang *et al.*, J. Nanosci. Nanotechnol. **11**, 5645 (2011).

[16] R. Y. Hong, B. Feng, L. L. Chen, G. H. Liu and H. Z. Li *et al.*, Biochem. Eng. J. **42**, 290 (2008).

[17] S. Hong, Y. Chang and I. Rhee, J. Korean Phys. Soc. **56**, 868 (2010).

[18] Y. Iqbal, H. Bae, I. Rhee and S. Hong, J. Nanosci. Nonotechnol. **16**, 11862 (2016).

[19] H. Bae, T. Ahmad, I. Rhee, Y. Chang and S. Jin *et al.*, Nano. Res. Lett. **7**, 44 (2012).

[20] T. Ahmad, H. Bae, I. Rhee, Y. Chang and S. Jin *et al.*, J. Nanosci. Nonotechnol. **12**, 5132 (2012).

[21] J. Lin, W. Zhou, A. Kumbhar, J. Wiemann and J. Fang *et al.*, J. Solid State Chem. **159**, 26 (2001).

[22] M. Khalkhali, S. Sadighian, K. Rostamizadeh, F. Khoeini and M. Naghibi *et al.*, Bioimpacts **5**, 141 (2015).

[23] M. M. Yallapu, M. Jaggi and S. C. Chauhan, Colloids Surf. B Biointerfaces **79**, 113 (2010).

[24] F. N. Sayed and V. Polshettiwar, Sci. Rep. **5**, 9733 (2015).

[25] V. Závišová, N. Tomašovičová, J. Kováča, M. Koneracká and P. Kopčanský *et al.*, in *Proceedings of NANOCON 2010* (Olomouc, Czech Republic, EU).

[26] Y. Okuhata, Adv. Drug Deliv. Rev. **37**, 121 (1999).